# Light Scattering from Filaments

Arno Zinke and Andreas Weber, *Member*, *IEEE*

**Abstract**—Photo realistic visualization of a huge number of individual filaments like in the case of hair, fur, or knitwear is a challenging task: Explicit rendering approaches for simulating radiance transfer at a filament get totally impracticable with respect to rendering performance and it is also not obvious how to derive efficient scattering functions for different levels of (geometric) abstraction or how to deal with very complex scattering mechanisms. We present a novel uniform formalism for light scattering from filaments in terms of radiance, which we call the Bidirectional Fiber Scattering Distribution Function (BFSDF). We show that previous specialized approaches, which have been developed in the context of hair rendering, can be seen as instances of the BFSDF. Similar to the role of the BSSRDF for surface scattering functions, the BFSDF can be seen as a general approach for light scattering from filaments, which is suitable for deriving approximations in a canonic and systematic way. For the frequent cases of distant light sources and observers, we deduce an efficient far field approximation (Bidirectional Curve Scattering Distribution Function, BCSDF). We show that on the basis of the BFSDF, parameters for common rendering techniques can be estimated in a non-ad-hoc, but physically-based way.

**Index Terms**—Three-dimensional graphics and realism—shading, light scattering, hair modeling, cloth modeling.

## 1 Introduction

Physically-based visualization of filaments like hair, fur, yarns, or grass can drastically improve the quality of a rendering in terms of photo realism. As long as the light transport mechanisms for light scattering are understood, rendering a single filament is usually not very challenging. In this case, the filament could be basically modeled by long and thin volumes having specific optical properties like the index of refraction or absorption coefficient. However, for the frequent case of a scene consisting of a huge number of individual fibers (like hair, fur, or knitwear) this explicit approach becomes impracticable with respect to rendering performance. It is also not clear a priori how to deal with very complex or unknown scattering mechanisms or how efficient visualizations of fibers based on measurement data could be implemented.

Although progress has been made in rendering particular fibers with particular lighting settings, no general formulation has been found. As a result, some more or less accurate models for specific fibers and illumination conditions were developed, especially in the realm of hair rendering [1], [2], [3], [4], [5]. If the viewing or lighting conditions change, such models may fail or have to be adopted.

### 1.1 Our Contribution

#### 1.1.1 Introduction of a Novel General Concept for Radiance Transfer at a Fiber

In this paper, we introduce a novel concept similar to Bidirectional Scattering-Surface Reflectance Distribution Functions (BSSRDF) and Bidirectional Scattering Distribution Functions (named BSDF) for surfaces in order to describe the radiance transfer at a fiber. The basic idea is to locally approximate this radiance transfer by a scattering function on the minimum enclosing cylinder of a straight infinite fiber, which is a first order approximation with respect to the curvature of the filament. We call this approximation a Bidirectional Fiber Scattering Distribution Function (BFSDF), which can be seen as a special BSSRDF that is not defined on the surface, but on the fiber's local minimum enclosing cylinder (see Section 4).

#### 1.1.2 Systematic Derivation of Less Complex Scattering Functions

Based on the BFSDF, we then derive further less complex scattering functions for different levels of (geometric) abstraction and for special lighting conditions, see Fig. 1. With the help of such scattering functions, efficient physically-based visualizations—adapted to a desired rendering technique or quality—are possible. Furthermore, the BFSDF allows for systematic comparisons and classifications of fibers with respect to their scattering distributions, since it provides a uniform and shape-independent radiance parameterization for filaments (see Sections 5, 6, and 7).

#### 1.1.3 General Framework for Existing Models for Hair Rendering

Moreover, we show that the existing models developed for hair rendering [1], [2] can be integrated in our framework, which also gives a basis to discuss their physical plausibility (see Section 8).

#### 1.1.4 Derivation of Analytical Solutions and Approximations for Special Cases

We furthermore address some special cases where analytical solutions or approximations are available, e.g., a general BCSDF for opaque fibers (mapped with a BRDF) is derived. In this context, we also derive a flexible and efficient near field shading model for dielectric fibers that accurately reproduces the scattering pattern for close ups but can be computed much more efficiently than the particle tracing (or an equivalent) that was typically used to capture the scattering pattern correctly (see Section 9).

#### 1.1.5 Integration into Existing Rendering Systems

We are able to propose approximations of the BFSDF, which translate it to some position-dependent BSDF and preserves

• *The authors are with the Institut für Informatik II, Universität Bonn, Römerstr. 164, 53117 Bonn, Germany.*
*E-mail: {zinke, weber}@cs.uni-bonn.de.*

*Manuscript received 7 Feb. 2006; revised 1 June 2006; accepted 14 June 2006; published online 10 Jan. 2007.*
*For information on obtaining reprints of this article, please send e-mail to: tvcg@computer.org, and reference IEEECS Log Number TVCG-0011-0206.*

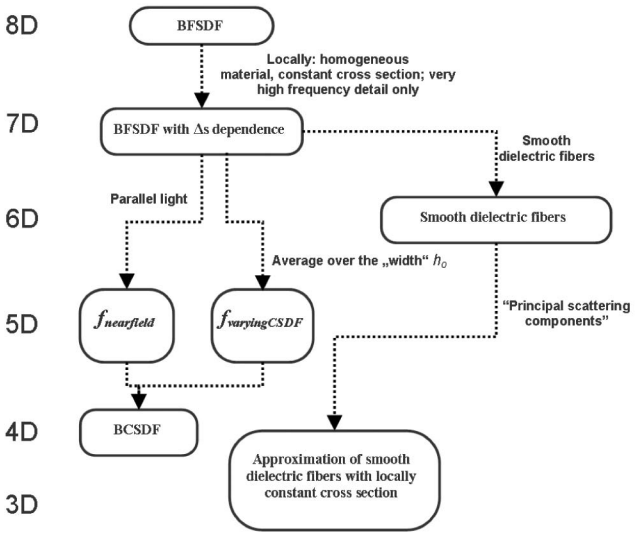


Fig. 1. Overview of the BFSDF and its special cases. The effective dimensions of the scattering functions are indicated on the left.

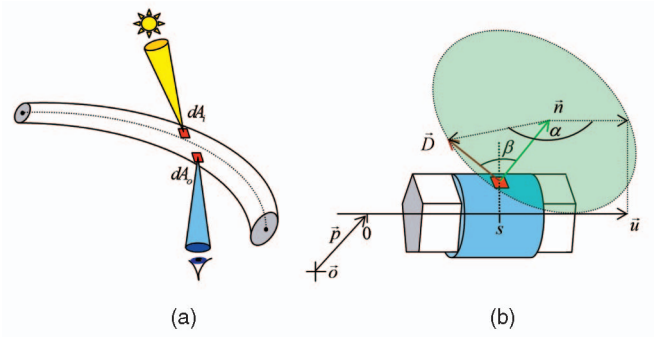


Fig. 2. (a) Incoming and outgoing radiance at a filament. (b) An "intuitive" variable set for parameterizing incoming and outgoing radiance at the minimum enclosing cylinder. In this example, the local cross section shape of the filament is pentagonal. The vector $\vec{u}$ denotes the local tangent (axis), $s$ the position along this axis. The angles $\alpha$ and $\beta$ span a hemisphere over the the surface patch at $s$, with $\alpha$ being measured with respect to $\vec{u}$ within the tangent plane and $\beta$ with respect to the local surface normal $\vec{n}$. Note that $\vec{D}$ represents both incoming and outgoing directions.

subtle scattering details, thus allowing an integration into existing rendering kernels that can cope with BSDF and polygons only (see Section 10).

## 2 Previous Work

Bidirectional Scattering Distribution Functions (BSDF) relate the incoming irradiance at an infinitesimal surface patch to the outgoing radiance from this patch [6]. It is an abstract optical material property which implies a constant wave length, a light transport taking zero time and being temporally invariant as well. Having the BSDF of a certain material, the local surface geometry, and the incoming radiance, the outgoing radiance can be reconstructed. This BSDF concept works well for a wide range of materials but has one major drawback: Incoming irradiance contributes only to the outgoing radiance from a patch, if it directly illuminates this patch. Therefore, it has to be generalized to take into account light transport inside the material. This generalization is called a Bidirectional Surface Scattering Distribution Function—BSSRDF [6]. Several papers have addressed some special cases mainly in the context of subsurface scattering [7], [8].

Further scattering models like BTF or even more generalized radiance transfer functions have been introduced to account for self-shadowing and other mesoscopic and macroscopic effects [9].

Marschner et al. [2] presented an approach specialized for rendering hair fibers. They very briefly introduce a novel curve scattering function defined with respect to curve intensity (intensity scattered per unit length of the curve) and curve irradiance (incoming power per unit length). Unfortunately, no hint about how it can be derived for other types of fibers than hair is given. One major restriction of the scattering model is that both viewer and light sources have to be distant to the hair fiber. Therefore, it is not suitable for rendering complex illumination like, for example, indirect illumination and hair-hair scattering, which are especially important for light colored hair [3]. Close-ups remain a problem, too. To fix those problems, the scattering model was extended to a specialized near field approach [3].

Another application of fiber rendering is the visualization of woven cloth, where optical properties of a single yarn have to be taken into account. A method for predicting a corresponding BSDF based on a certain weaving pattern and on dielectric fibers was developed by Volevich et al. [10]. Gröller et al. proposed a volumetric approach for modeling knitwear [11]. They first measure the statistical density distribution of the cross section of a single yarn with respect to the arrangement of individual yarn fibers and then translate it along a three-dimensional curve to form the entire filament. The results are looking quite impressive, but the question of how to deal with yarns with more complex scattering properties is not addressed. A similar idea was presented by [12]. Here, all computations are based on a structure called lumislice, a light field for a yarn-cross-section. However, the authors do not address the problem of computing a physically-based light field according to the properties of a single fiber of the yarn.

Adabala et al. [13] describe another method for visualizing woven cloth. Due to the limitations of the underlying BRDF (Cook-Torance microfacet BRDF), realistic renderings of yarns with more complex scattering properties remain a problem. In the realm of applied optics, light scattering from straight smooth dielectric fibers with constant and mainly circular or elliptical cross sections were analyzed in a number of publications [14], [15], [16], [17], [18]. Schuh and Wriedt [19] introduced an approximation which is capable of predicting scattering of electromagnetic waves from curved fibers, too. All these approaches are of very high quality, but are either more specialized in predicting the maxima positions of the scattering distribution or rather impractical for rendering purposes because of their high numerical complexity.

## 3 Basics and Notations

### 3.1 Motivation and General Assumptions

We want to apply the basics of the radiometric concepts for surfaces in the realm of fiber optics. The general problem is very similar: How much radiance $\mathrm{d}L_o$ scattered from a single fiber one would observe from an infinitesimal surface patch $\mathrm{d}A_o$ in direction $(\alpha_o, \beta_o)$, if a surface patch $\mathrm{d}A_i$ is illuminated by an irradiance $E_i$ from direction $(\alpha_i, \beta_i)$ (see Fig. 2a).

This interrelationship could be basically described by a BSSRDF at the surface of the fiber. Such a BSSRDF would, in general, depend on macroscopic deformations of the fiber, such as how the fiber is oriented and warped. As a consequence, local (microscopic) fiber properties could not be separated from their global macroscopic geometry. Furthermore, all radiometric quantities must be parameterized with respect to the actual surface of the filament, which may not be well defined—as, e.g., in the case of a fluffy wool yarn.

Therefore, we define a BSSRDF on the local infinite minimum enclosing cylinder rather than on the actual surface of the fiber in order to make the parameterization independent of the fiber's geometry. Thus, the radiance transfer at the fiber is locally approximated by a scattering function on the minimum enclosing cylinder of a straight infinite fiber, which means a first order approximation with respect to the curvature. We call this function a Bidirectional Fiber Scattering Distribution Function (BFSDF). This approximation is accurate if the influence of curvature to the scattering distribution can be neglected. This is the case, e.g., if

- the filament's curvature is small compared to the radius of its local minimum enclosing cylinder, or
- most of the incoming radiance only locally contributes to outgoing radiance.

The latter condition is satisfied, for instance, by opaque wires, since only reflection occurs and, therefore, no internal light transport inside the filament takes place. Hence, the scattering is a purely local phenomenon and the curvature of the fiber plays no role at all. The former condition, for instance, holds for hair and fur. In this case, substantial internal light transport takes place, but since the curvature is small compared to the radius and since the light gets attenuated inside the fiber, the differences compared to a straight infinite fiber may be neglected. The higher the curvature and the more internal light transport takes place, the bigger the potential error that is introduced by the BFSDF.

### 3.2 Notations

Before technically defining the BFSDF, we will give an overview of our notations, which follow [2] in general.

The local filament axis is denoted $\vec{u}$ and we refer to the planes perpendicular to $\vec{u}$ as normal planes. All local surface normals lie within the local normal plane. All incoming and outgoing radiance is parameterized with respect to the local minimum enclosing cylinder with radius $r$ oriented along $\vec{u}$ and is therefore independent of the actual cross section geometry of the filament (Fig. 3a).

We introduce two sets of variables, which are suitable for certain measurement or lighting settings. The first parameter set describes every infinitesimal surface patch $\mathrm{d}A$ at the enclosing cylinder by its tangential position $s$ and its azimuthal position $\xi$ within the normal plane (cylindrical coordinates). The directions of both incoming and outgoing radiance are then given by two spherical angles $\alpha$ and $\beta$ which span a hemisphere at $\mathrm{d}A$ oriented along the local surface normal of the enclosing cylinder (Figs. 2b and 3b).

Typically, this very intuitive way to parameterize both directions and positions is not very well suited to actual problems. In particular, this is the case for data acquisition and many "real-world" lighting conditions. Hence, we introduce a second set of variables according to [2]. This set can be split into two groups, one parameterizing all azimuthal features within the normal plane $(h, \varphi)$ and another parameterizing all longitudinal features $(s, \theta)$. The angle $\theta$ denotes the inclination of a direction with respect to the normal plane, $\varphi$ its azimuthal angle with respect to a fixed axis $\vec{v}$, and $h$ an offset position of the surface patch at the minimum enclosing cylinder measured within the normal plane. The variable $s$ is the same as introduced before and always means the position along the axis of the minimum enclosing cylinder (Fig. 3).

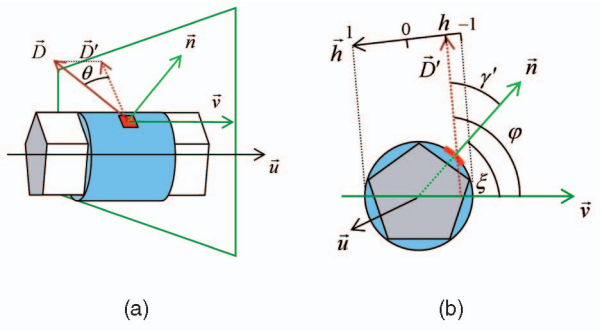


Fig. 3. (a) Parameterization with respect to the normal plane and filament axis (tangent) $\vec{u}$. The vector $\vec{D}'$ denotes the projection of a direction $\vec{D}$ onto the normal plane. The angle $\theta$ ranges from $-\pi/2$ to $\pi/2$, with $\theta = \pi/2$ if $\vec{u}$ and $\vec{D}$ are pointing in the same direction. (b) Azimuthal variables within the normal plane. The parameter $h$ is an offset position at the perimeter. Note that parallel rays have same $\varphi$ (measured counterclockwise with respect to $\vec{u}$) but different $h$.

We will now derive some useful transformation formulae for variables of both sets.

The projection of the angle of incidence at the enclosing cylinder onto the normal plane $\gamma'$ is given by the following two equations:

$$\cos\gamma' = \frac{\cos\beta}{\cos\theta}, \tag{1}$$

$$\gamma' = |\arcsin h|. \tag{2}$$

Thus, for the spherical angle $\beta$, we have

$$\beta = \arccos(\cos\theta\sqrt{1-h^2}). \tag{3}$$

The following relation holds between $\xi$, $\varphi$, and $h$, see Fig. 3:

$$\xi = \begin{cases} \varphi + \arcsin h & 0 \le \varphi + \arcsin h < 2\pi \\ 2\pi + \varphi + \arcsin h & \varphi + \arcsin h < 0 \\ \varphi + \arcsin h - 2\pi & \varphi + \arcsin h \ge 2\pi. \end{cases} \tag{4}$$

The spherical coordinate $\alpha$ equals the angle between the projection of $\vec{D}$ onto the local tangent plane and $\vec{v}$. Since the angle between $\vec{D}$ and $\vec{v}$ is given by $\pi/2 - \theta$ and the inclination of $\vec{D}$ with respect to the tangent plane is $\pi/2 - \beta$, one obtains:

$$\begin{aligned} \cos\alpha &= \cos(\pi/2-\theta)/\cos(\pi/2-\beta) \\ &= \sin\theta/\sin\beta \\ &= \frac{\sin\theta}{\sqrt{1-(1-h^2)\cos^2\theta}}. \end{aligned} \tag{5}$$

Furthermore, the actual angle depends on the sign of $h$:

$$\alpha = \begin{cases} \arccos\left(\frac{\sin\theta}{\sqrt{1-(1-h^2)\cos^2\theta}}\right), & h \le 0, \\ 2\pi - \arccos\left(\frac{\sin\theta}{\sqrt{1-(1-h^2)\cos^2\theta}}\right), & h > 0. \end{cases} \tag{6}$$

## 4 Bidirectional Fiber Scattering Distribution Function—BFSDF

We now technically define the **B**idirectional **F**iber **S**cattering **D**istribution **F**unction (BFSDF) of a fiber. The BFSDF relates incident flux $\Phi_i$ at an infinitesimal surface patch $\mathrm{d}A_i$ to the outgoing radiance $L_o$ at another position on the minimum enclosing cylinder:

$$f_{\mathrm{BFSDF}}(s_i,\xi_i,\alpha_i,\beta_i,s_o,\xi_o,\alpha_o,\beta_o) := \frac{\mathrm{d}L_o(s_i,\xi_i,\alpha_i,\beta_i,s_o,\xi_o,\alpha_o,\beta_o)}{\mathrm{d}\Phi_i(s_i,\xi_i,\alpha_i,\beta_i)}. \tag{7}$$

Using the BFSDF, the local orientation of a fiber, and the incoming radiance $L_i$, the total outgoing radiance of a particular position can be calculated by integrating the irradiance over all surface patches and all incoming directions as follows:

$$L_o(s_o,\xi_o,\alpha_o,\beta_o) = \int_{-\infty}^{+\infty}\int_0^{2\pi}\int_0^{2\pi}\int_0^{\pi/2} f_{\mathrm{BFSDF}}(s_i,\xi_i,\alpha_i,\beta_i,s_o,\xi_o,\alpha_o,\beta_o) \tag{8}$$
$$L_i(s_i,\xi_i,\alpha_i,\beta_i)\,\sin\beta_i\,\cos\beta_i\,\mathrm{d}\beta_i\,\mathrm{d}\alpha_i\,\mathrm{d}\xi_i\,\mathrm{d}s_i.$$

For physically-based BFSDF, the energy is conserved, thus all light entering the enclosing cylinder is either absorbed or scattered. In case of perfectly circular symmetric filaments, the BFSDF in addition satisfies the Helmholtz Reciprocity:

$$f_{\mathrm{BFSDF}}(s_i,\xi_i,\alpha_i,\beta_i,s_o,\xi_o,\alpha_o,\beta_o) = f_{\mathrm{BFSDF}}(s_o,\xi_o,\alpha_o,\beta_o,s_i,\xi_i,\alpha_i,\beta_i). \tag{9}$$

If the optical properties of a fiber are constant along $s$, then the BFSDF does not depend on $s_i$ and $s_o$ but on the difference $\Delta s := s_o - s_i$. Thus, the dimension of the BFSDF function decreases by one and the scattering integral reduces to the following equation:

$$L_o(s_o,\xi_o,\alpha_o,\beta_o) = \int_{-\infty}^{+\infty}\int_0^{2\pi}\int_0^{2\pi}\int_0^{\pi/2} f_{\mathrm{BFSDF}}(\Delta s,\xi_i,\alpha_i,\beta_i,\xi_o,\alpha_o,\beta_o) \tag{10}$$
$$_i(s_i,\xi_i,\alpha_i,\beta_i)\,\sin\beta_i\,\cos\beta_i\,\mathrm{d}\beta_i\,\mathrm{d}\alpha_i\,\mathrm{d}\xi_i\,\mathrm{d}\Delta s.$$

This special case is an appropriate approximation for the general case if the following condition is satisfied:

- The cross section shape and material properties vary slowly or at a very high frequency with respect to $s$.

Good examples for high frequency detail are cuticula tiles of hair fibers or surface roughness due to the microstructure of a filament. Since the latter assumption is at least locally valid for a wide range of different fibers, we will restrict ourselves to this case in the following.

The BFSDF and its corresponding rendering integral was introduced with respect to the "intuitive variable set" first. We now derive a formulation for the second variable set. Reparameterizing the scattering integral yields:

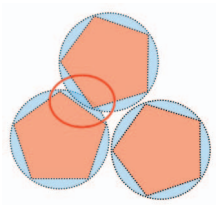

Fig. 4. Cross section of three very densely packed fibers. The problematic intersection of two enclosing cylinders is marked by an ellipse.

$$L_o(s_o,h_o,\varphi_o,\theta_o) = \int_{-\infty}^{+\infty}\int_{-1}^{1}\int_0^{2\pi}\int_{-\pi/2}^{\pi/2} \left|\frac{\partial(\xi_i,\alpha_i,\beta_i)}{\partial(h_i,\varphi_i,\theta_i)}\right| f_{\mathrm{BFSDF}}(\Delta s,h_i,\varphi_i,\theta_i,h_o,\varphi_o,\theta_o) L_i(s_i,h_i,\varphi_i,\theta_i) \sqrt{1-\cos^2\theta_i(1-h_i^2)}\sqrt{1-h_i^2}\cos\theta_i\,\mathrm{d}\theta_i\,\mathrm{d}\varphi_i\,\mathrm{d}h_i\,\mathrm{d}\Delta s. \tag{11}$$

The above equation can be finally simplified to the following equation:

$$L_o(s_o,h_o,\varphi_o,\theta_o) = \int_{-\infty}^{+\infty}\int_{-1}^{1}\int_0^{2\pi}\int_{-\pi/2}^{\pi/2} f_{\mathrm{BFSDF}}(\Delta s,h_i,\varphi_i,\theta_i,h_o,\varphi_o,\theta_o) \cos^2\theta_i L_i(s_i,h_i,\varphi_i,\theta_i)\,\mathrm{d}\theta_i\,\mathrm{d}\varphi_i\,\mathrm{d}h_i\,\mathrm{d}\Delta s. \tag{12}$$

This form of the scattering integral is especially suitable when having distant lights, i.e., parallel illumination, since parallel rays of light have the same $\varphi_i$ and $\theta_i$ but different $h_i$. Consider, for example, directional lighting, which can be expressed by the radiance distribution $L(\varphi_i',\theta_i',\varphi_i,\theta_i) = E_\perp(\varphi_i',\theta_i')\delta(\varphi_i-\varphi_i')\delta(\theta_i-\theta_i')/\cos\theta_i$ with normal irradiance $E_\perp(\varphi_i',\theta_i')$. Substituting the radiance in the scattering integral by this distribution yields:

$$L_o(h_o,\varphi_o,\theta_o) = E_\perp(\varphi_i',\theta_i')\cos\theta_i' \int_{-\infty}^{+\infty}\int_{-1}^{1} f_{\mathrm{BFSDF}}(\Delta s,h_i,\varphi_i',\theta_i',h_o,\varphi_o,\theta_o)\mathrm{d}h_i\mathrm{d}\Delta s. \tag{13}$$

All formulae derived in this section hold for a single filament only. But, a typical scene consists of a huge number of densely packed fiber assemblies. Since incoming and outgoing radiance was parameterized with respect to the minimum enclosing cylinder, those cylinders must not intersect. Otherwise, it cannot be guaranteed that the results are still valid (Fig. 4). If a cross section shape closely matches the enclosing cylinder, the maximum overlap is very small. Hence, computing the light transport at a projection of the overlapping regions onto the enclosing cylinder can be seen as a good approximation of the actual scattering.

## 5 Dielectric Fibers

Since most filaments consist of dielectric material, it is very instructive to discuss the scattering at dielectric fibers. For perfectly smooth dielectric filaments with arbitrary, but, constant, cross section, the dimension of the BFSDF reduces from seven to six. This is a direct consequence of the fact that

light entering at a certain inclination will always exit at the same inclination (according to absolute value), regardless of the sequence of refractions and reflections it undergoes.

The incident light is reflected or refracted several times before it leaves the fiber. The amount of light being reflected, respectively, refracted, is given by Fresnel's Law. At each surface interaction step, the scattered intensity of a ray decreases—except in case of total reflection. If absorption inside the fiber takes place, then loss of energy is even more prominent. Since an incoming ray of light does not exhibit spatial or angular blurring, the BFSDF is characterized by discrete peaks. Therefore, it makes sense to analyze only those scattering components with respect to their geometry and attenuation which

- can be measured outside the fiber and
- have an intensity bigger than a certain given threshold.

As a result, the BFSDF can be approximated very well by the distribution of the strongest peaks. Then, the effective complexity further reduces to three dimensions since all scattering paths and, thereby, all scattering components, are fully determined by $h_i$, $\varphi_i$, and $\theta_i$ which are needed to compute the attenuation.

Having $n$ such components, the BFSDF may be factorized:

$$\begin{aligned} & f_{\mathrm{BFSDF}}(\Delta s, h_i, \varphi_i, \theta_i, h_o, \varphi_o, \theta_o) \\ & \quad \approx \sum_{j=1}^{n} f^j_{\mathrm{BFSDF}}(\Delta s, h_i, \varphi_i, \theta_i, h_o, \varphi_o, \theta_o) \\ & \quad = \frac{\delta_\theta(\theta_i + \theta_o)}{\cos^2\theta_i} \sum_{j=1}^{n} \delta^j_s\Big(\Delta s - \lambda^j_s(h_o, \varphi_o, \theta_o)\Big) \\ & \qquad \delta^j_\varphi\Big(\varphi_i - \lambda^j_\varphi(h_o, \varphi_o, \theta_o)\Big) \\ & \qquad \delta^j_h\Big(h_i - \lambda^j_h(h_o, \varphi_o, \theta_o)\Big) \\ & \qquad a^j(h_o, \varphi_o, \theta_o). \end{aligned} \tag{14}$$

The first factor $\delta_\theta$ says that intensity can only be measured if $\theta_o = -\theta_i$. Since no blurring of the scattered ray of light occurs, all other factors describing the scattering geometry are formalized by Dirac delta distributions too. Because rays entering the enclosing cylinder at $s_i$ propagate into longitudinal direction, they usually exit the enclosing cylinder at another longitudinal position $s$. The functions $\lambda^j_s$ account for this relationship between $s_i$ and $s$. The two functions $\lambda^j_\varphi$ and $\lambda^j_h$ characterize the actual scattering geometry (the paths of the projection of the ray paths onto the normal plane). The factor $a^j$ is the attenuation for the $j$th component. These attenuation factors include Fresnel factors as well as absorption. Due to the Bravais Law [2], all $\lambda^j$ and $a^j$ can be directly derived from the 2D analysis of the optics of cross section of a fiber within the normal plane together with a modified index of refraction (depending on the incoming inclination $\theta_i$, see the next section).

Note that the factor $(\cos\theta_i)^{-2}$ in front of the equation compensates for

- the integration measure with respect to $\theta_i$, $h_i$, and $\varphi_i$ which contributes a factor of $(\cos\theta_i)^{-1}$ and
- the cosine of the angle of incidence which gives another $(\cos\theta_i)^{-1}$.

Even though this kind of BFSDF is for smooth dielectric materials with absorption and locally constant cross section only, its basic structure is very instructive for a lot of other types of fibers too. For example, internal volumetric scattering or surface scattering—due to surface roughness—do not change this basic structure in most cases but result in spatial and angular blurring, see Fig. 7. By replacing the $\delta$-distributions in the BFSDF for smooth dielectric cylinders—see (15)—with normalized lobes (like Gaussians) centered over the peak similar effects can be simulated easily.

The presence of sharp peaks in the scattering distribution is not only a characteristic of dielectric fibers with constant cross section, but of most other types of (even not dielectric) fibers with locally varying cross section shape too. If the variation is periodic and of a very high frequency, these peaks are typically shifted or blurred in longitudinal directions, compared to a fiber without this high-frequency detail. Nevertheless, the Bravais Law only holds for constant cross sections. Hence, (14) has to be adopted to other cases. At least it can be seen as a basis for efficient compression schemes and as a starting point for analytical BFSDFs.

### 5.1 Dielectric Cylinders

As an interesting analytical example—which was already partially discussed in [14], [19], and [2]—we now analyze the scattering of a cylindric fiber made of colored dielectric material with radius $r$. We restrict ourselves to the first three scattering components (Fig. 6) dominating the visual appearance and denote them according to [2]:

- The first backward scattering component, which is a direct (white) surface reflection (R-component).
- The first forward scattering component, which is light that is transmitted two times through the cylinder (TT-component).
- The second backward scattering component, which is light which enters the cylinder and gets internally reflected (TRT-component).

Hence, the resulting BFSDF is a superposition of three independent scattering functions, each accounting for one of the three modes:

$$\begin{aligned} & f^{\mathrm{cylinder}}_{\mathrm{BFSDF}} \approx \\ & \quad \frac{\delta_\theta}{\cos^2\theta_i}\Big(\delta^{\mathrm{R}}_s\delta^{\mathrm{R}}_\varphi\delta^{\mathrm{R}}_h a^{\mathrm{R}} + \delta^{\mathrm{TT}}_s\delta^{\mathrm{TT}}_\varphi\delta^{\mathrm{TT}}_h a^{\mathrm{TT}} \\ & \qquad + \delta^{\mathrm{TRT}}_s\delta^{\mathrm{TRT}}_\varphi\delta^{\mathrm{TRT}}_h a^{\mathrm{TRT}}\Big). \end{aligned} \tag{15}$$

Neglecting the attenuation factors $a^{\mathrm{R}}$, $a^{\mathrm{TT}}$, and $a^{\mathrm{TRT}}$, this BFSDF can be derived by tracing the projections of rays within the normal plane (Fig. 6a). Rays entering the cylinder at an offset $h_i$ always exit at $-h_i$. Furthermore, intensity can only be measured if the relative azimuth $\varphi = M[\varphi_o - \varphi_i]$ equals $\varphi_R$ for the R-component, $\varphi_{\mathrm{TT}}$ for the TT-component, or $\varphi_{\mathrm{TRT}}$ for the TRT-component. Here, the operator $M$ maps the difference angle $\varphi_o - \varphi_i$ to an interval $(-\pi, \pi]$:

$$M[\alpha] = \begin{cases} \alpha, & -\pi < \alpha \le \pi \\ \alpha - 2\pi, & \pi < \alpha \le 2\pi \\ \alpha + 2\pi, & -2\pi \le \alpha \le -\pi. \end{cases} \tag{16}$$

For the relative azimuths, the following equations hold, see Fig. 6a:

$$\varphi_{\mathrm{R}} = 2\gamma_i', \tag{17}$$
$$\varphi_{\mathrm{TT}} = M[\pi + 2\gamma_i' - 2\gamma_t'], \tag{18}$$
$$\varphi_{\mathrm{TRT}} = 2\gamma_i' - 4\gamma_t'. \tag{19}$$

Due to the Bravais Law, all azimuths are calculated from a 2D-scattering within the normal plane with the help of a modified index of refraction

$$n' = \frac{\sqrt{n^2 - \sin^2\theta_i}}{\cos\theta_i}$$

(instead of the relative refractive index $n$) and Snell's Law [2]. The projected (signed) angle of incidence light is denoted $\gamma_i'$ and equals $\arcsin h_i$. Its corresponding (signed) angle of refraction is $\gamma_t' = \arcsin(h_i/n')$.

Because rays entering the cylinder at a position $s_i$ propagate into a longitudinal $s$-direction, they leave the fiber at other positions $s_{\mathrm{TT}}$ and $s_{\mathrm{TRT}}$, respectively. In case of direct surface reflection (R-mode), the light is reflected at incoming position $s_i$. The two positions, $s_{\mathrm{TT}}$ and $s_{\mathrm{TRT}}$, are directly related to the length covered by the ray inside the cylinder. For the TT component, this length $l$ can be calculated from its projection onto the normal plane $l_s$ and the longitudinal angle of refraction $\theta_t$ (see Fig. 6):

$$l = \frac{l_s}{\cos\theta_t} = \frac{2r\,\cos\gamma_t'}{\cos\theta_t} \tag{20}$$

with $\theta_t = -\mathrm{sgn}(\theta_i)\arccos((n'/n)\cos\theta_i)$. This length doubles for rays of the TRT-mode.

Therefore, for the positions $s_{\mathrm{TT}}$ and $s_{\mathrm{TRT}}$, the following holds:

$$s_{\mathrm{TT}} = -\mathrm{sgn}\theta_i\sqrt{l^2 - l_s^2} = l_s\tan\theta_t, \tag{21}$$
$$s_{\mathrm{TRT}} = 2l_s\tan\theta_t. \tag{22}$$

Putting all geometric analysis together, the geometry terms $\lambda$ introduced in the previous section are:

$$\begin{aligned}
&\lambda_s^{\mathrm{R}} = 0; \lambda_s^{\mathrm{TT}} = s_{\mathrm{TT}}; \lambda_s^{\mathrm{TRT}} = s_{\mathrm{TRT}},\\
&\lambda_h^{\mathrm{R}} = \lambda_h^{\mathrm{TT}} = \lambda_h^{\mathrm{TRT}} = -h_o,\\
&\lambda_\varphi^{\mathrm{R}} = \varphi_o + 2\arcsin h_o,\\
&\lambda_\varphi^{\mathrm{TT}} = \varphi_o + M[\pi + 2\arcsin(h_o) - 2\arcsin(h_o/n')],\\
&\lambda_\varphi^{\mathrm{TRT}} = \varphi_o - 4\arcsin(h_o/n') + 2\arcsin h_o.
\end{aligned} \tag{23}$$

For smooth dielectric cylinders, the R component gets attenuated by Fresnel reflectance only:

$$a^{\mathrm{R}} = \mathrm{Fresnel}(n', \tilde{n}', \gamma_i'). \tag{24}$$

According to [2], the index $n'$ is used to calculate the reflectance for perpendicular polarized light, whereas another index of refraction $\tilde{n}' = n^2/n'$ is used for parallel polarized light.

For the two other modes (TT, TRT), a ray gets attenuated at each reflection, respectively, refraction event. Hence, for the corresponding Fresnel factors $\mathrm{Fresnel}_{\mathrm{TT}}$ and $\mathrm{Fresnel}_{\mathrm{TRT}}$, the following equations hold:

$$\mathrm{Fresnel}_{\mathrm{TT}} = (1 - a^{\mathrm{R}})(1 - \mathrm{Fresnel}(1/n', 1/\tilde{n}', \gamma_t')), \tag{25}$$

$$\mathrm{Fresnel}_{\mathrm{TRT}} = \mathrm{Fresnel}_{\mathrm{TT}}\mathrm{Fresnel}(1/n', 1/\tilde{n}'', \gamma_t'). \tag{26}$$

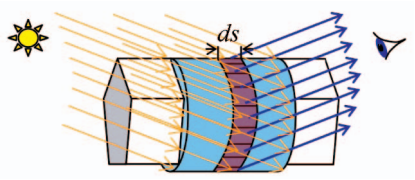


Fig. 5. A slice at the minimum enclosing cylinder illuminated by parallel light and viewed by a distant observer.

If a ray enters the cylinder, as is the case for both the TT and TRT modes, absorption takes places. For homogenous materials, the attenuation only depends on the length of the internal path—i.e., the absorption length—and the absorption coefficient $\sigma$, which is a wavelength-dependent material parameter. For the TT component, the absorption length equals $l$ and a ray of the TRT mode covers twice this distance inside the cylinder. Note that the absorption length given in [2] (which was $l = (2 + 2\cos\gamma_t')/\cos\theta_t$) is wrong.

Hence, the total attenuation factors with absorption are

$$a^{\mathrm{TT}} = \mathrm{Fresnel}_{\mathrm{TT}}\, e^{-\sigma l}, \tag{27}$$

$$a^{\mathrm{TRT}} = \mathrm{Fresnel}_{\mathrm{TRT}}\, e^{-2\sigma l}. \tag{28}$$

Note that higher order scattering can be analyzed in a straightforward way since analytical solutions for the corresponding geometry terms $\lambda$ are available.

## 6 Far Field Approximation and BCSDF

"Real-world" filaments are typically very thin and long structures. Hence, compared to its effective diameter both viewing and lighting distances are typically very large. Therefore, all surface patches along the normal plane have equal ($\varphi_o$, $\theta_o$) and the fibers cross section is locally illuminated by parallel light (of constant radiance) from a fixed direction ($\varphi_i$, $\theta_i$). Furthermore, adjacent surface patches of the local minimum enclosing cylinder have nearly the same distance to both light source and observer.

When rendering such a scene the screen space width of a filament is less or in the order of magnitude of a single pixel. In this case, fibers can be well approximated by curves having a cross section proportional to the diameter of the minimum enclosing cylinder $D$.

That allows us to introduce a simpler scattering formalism to further reduce rendering complexity which we call far field approximation, see [3].

Using similar quantities as Marschner et al. [2] (curve radiance and curve irradiance), we show how an appropriate scattering function can be derived right from the BFSDF. The *curve radiance* $\mathrm{d}\bar{L}_o$ is the averaged outgoing radiance along the width of the fibers minimum enclosing cylinder times its effective diameter (Fig. 5).

Assuming parallel light from direction ($\varphi_i$, $\theta_i$) being constant over the width of a fiber, this curve radiance can be computed by averaging the outgoing radiance of all visible patches at $s_o$ (over the width of the fiber) and weighting them with respect to their relative screen space coverage (projected area to screen space) by a factor of $\cos(\xi_o - \varphi_o)$:

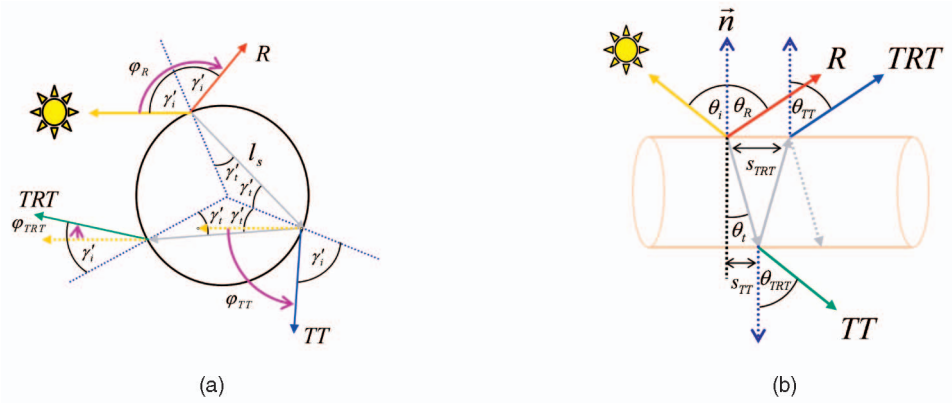


Fig. 6. (a) Azimuthal scattering geometry of the first three scattering modes (R, TT, TRT) within the normal plane for a fiber with circular cross section. The relative azimuths are denoted $\varphi_R$, $\varphi_{TT}$, and $\varphi_{TRT}$. Here, the projection of the angle of incidence onto the normal plane is $\gamma_i'$ and the angle of refraction is $\gamma_r'$, respectively. Note that the outgoing ray leaves the fiber always at $-h_i$. (b) Longitudinal scattering geometry of the first three scattering modes (R, TT, TRT) at a dielectric fiber. Note that the outgoing inclinations $\theta_R$, $\theta_{TT}$, and $\theta_{TRT}$ always equal $-\theta_i$. The difference of the longitudinal outgoing positions with respect to incoming position $s_i$ are denoted $s_{\mathrm{R}}$, $s_{\mathrm{TT}}$, and $s_{\mathrm{TRT}}$.

$$\mathrm{d}\bar{L}_o(\varphi_i,\theta_i,\varphi_o,\theta_o) := \frac{D}{\pi}\int_{\varphi_o-\pi/2}^{\varphi_o+\pi/2}\cos(\xi_o-\varphi_o)\,\mathrm{d}L_o(\varphi_i,\theta_i,\xi_o,\alpha_o(\theta_o,h_o(\xi_o,\varphi_o)),\beta_o(\theta_o,h_o(\xi_o,\varphi_o)))\mathrm{d}\xi_o. \tag{29}$$

Notice that, for the integration with respect to $\xi_o$, one has to take into account its transition from zero to $2\pi$ properly. Alternatively, one gets the following equation by integration with respect to $h$:

$$\mathrm{d}\bar{L}_o(\varphi_i,\theta_i,\varphi_o,\theta_o) = \frac{D}{2}\int_{-1}^{1}\mathrm{d}L_o(h_o,\varphi_i,\theta_i,\varphi_o,\theta_o)\mathrm{d}h_o. \tag{30}$$

The factor $D$ amounts for the fact that the projected area to screen space is proportional to the width of a fiber.

Since we assume constant incident radiance $L_i(\varphi_i,\theta_i)$, $\mathrm{d}L_o$ may be substituted by:

$$\mathrm{d}L_o(\varphi_i,\theta_i,h_o,\varphi_o,\theta_o) = \cos^2\theta_i L_i(\varphi_i,\theta_i)\mathrm{d}\varphi_i\mathrm{d}\theta_i\mathrm{d}h_o \int_{-1}^{1}\int_{-\infty}^{\infty} f_{\mathrm{BFSDF}}(\Delta s,h_i,\varphi_i,\theta_i,h_o,\varphi_o,\theta_o)\,\mathrm{d}\Delta s\,\mathrm{d}h_i, \tag{31}$$

which yields:

$$\mathrm{d}\bar{L}_o(\varphi_o,\theta_o,\varphi_i,\theta_i) = \frac{D}{2}L_i(\varphi_i,\theta_i)\cos^2\theta_i\mathrm{d}\varphi_i\mathrm{d}\theta_i \int_{-1}^{1}\int_{-1}^{1}\int_{-\infty}^{\infty} f_{\mathrm{BFSDF}}(\Delta s,h_i,\varphi_i,\theta_i,h_o,\varphi_o,\theta_o)\,\mathrm{d}\Delta s\,\mathrm{d}h_i\mathrm{d}h_o. \tag{32}$$

This scattered radiance $\mathrm{d}\bar{L}_o$ is proportional to the incoming *curve irradiance* $\mathrm{d}\bar{E}_i$:

$$\mathrm{d}\bar{E}_i(\varphi_i,\theta_i) := DL_i(\varphi_i,\theta_i)\cos^2\theta_i\mathrm{d}\varphi_i\mathrm{d}\theta_i. \tag{33}$$

Thus, a new bidirectional far-field scattering distribution function for curves that assumes a distant observer and distant light sources can be defined. It relates the incoming curve irradiance to the averaged outgoing radiance along the the width (curve radiance). We will call it $f_{\mathrm{BCSDF}}$ (**B**idirectional **C**urve **S**cattering **D**istribution **F**unction):

$$f_{\mathrm{BCSDF}}(\varphi_i,\theta_i,\varphi_o,\theta_o) := \frac{\mathrm{d}\bar{L}_o(\varphi_o,\theta_o,L(\varphi_i,\theta_i))}{\mathrm{d}\bar{E}_i(\varphi_i,\theta_i)}. \tag{34}$$

By comparing (32) and (33), we obtain:

$$f_{\mathrm{BCSDF}}(\varphi_i,\theta_i,\varphi_o,\theta_o) = \frac{1}{2}\int_{-1}^{1}\int_{-1}^{1}\int_{-\infty}^{\infty} f_{\mathrm{BFSDF}}(\Delta s,h_i,\varphi_i,\theta_i,h_o,\varphi_o,\theta_o)\mathrm{d}\Delta s\,\mathrm{d}h_i\,\mathrm{d}h_o. \tag{35}$$

Finally, in order to compute the total outgoing curve radiance, one has to integrate all incoming light over a sphere with respect to $\varphi_i$ and $\theta_i$:

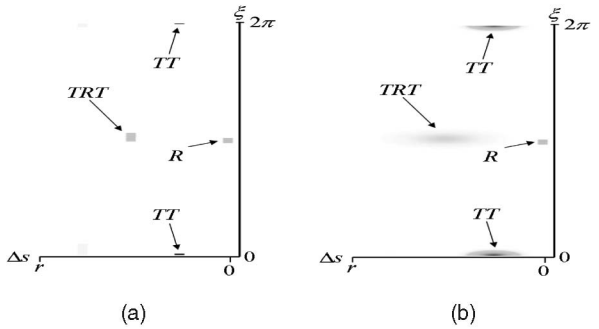


Fig. 7. (a) The diagram shows the distribution of scattered light at a perfect smooth dielectric circular cylinder obtained with particle tracing. The intensity of the scattered light is computed with respect to $\xi$ and $\Delta s$ at the cylindric shell: The darker the gray, the higher the outgoing flow through the surface. A single light source is illuminating a small rectangular surface patch at $s=0$ from direction $\varphi=\pi$ and $\theta=0.2$. The direct surface reflection component (R), the forward scattered component (TT), and the first order caustic (TRT) are clearly and sharply visible. (b) Shows the same scene but a dielectric cylinder with volumetric scattering. As a consequence, both TT and TRT components are blurred. Note that the structure of the scattering distribution (i.e., the position of the peaks and their relative intensities) does not change.

$$\bar{L}_o(\varphi_o,\theta_o) = D\int_0^{2\pi}\int_{-\pi/2}^{\pi/2} f_{\mathrm{BCSDF}}(\varphi_i,\theta_i,\varphi_o,\theta_o)L_i(\varphi_i,\theta_i)\cos^2\theta_i \mathrm{d}\theta_i\,\mathrm{d}\varphi_i. \tag{36}$$

This equation matches the rendering integral given in [2, (1)] in the specific context of hair rendering. Thus, the BCSDF is identical to the fiber scattering function very briefly introduced in [2]. In contrast to [2], our derivation shows the close connection between the BFSDF and the BCSDF. In our formalism, the BCSDF is just one specific approximation of the BFSDF and can be computed directly from (35).

Besides the advantage of being less complex than the BFSDF, the BCSDF can help to drastically reduce sampling artifacts which would be introduced by subtle BFSDF detail like very narrow scattering lobes. Nevertheless, there are some drawbacks. First of all, local scattering effects are neglected which restricts the possible fields of application of the BCSDF in case of close ups or indirect illumination. Furthermore, since the fiber properties are averaged over the width, the entire width (at least in the statistical average) has to be visible. Otherwise, undesired artifacts may occur. Finally, the BCSDF is not adequate for computing indirect illumination due to multiple fiber scattering in dense fiber clusters since the far field assumption is violated in this case.

## 7 Further Special Cases

Although a distant observer and distant light sources are commonly assumed for rendering, there may be cases where these two assumptions may be not valid. For those situations, further approximations of the BFSDF are straight forward and can be derived similarly to the BCSDF. In particular, we now discuss the following two special cases:

- A close observer and locally constant incident lighting: Near field scattering with constant incident lighting, and
- A distant observer with locally varying incident lighting: Curve scattering with locally varying incident lighting.

### 7.1 Near Field Scattering with Constant Incident Lighting

Although a BCSDF may be a good approximation for distant observers, it fails when it comes to close ups. Since the outgoing radiance is averaged with respect to the width of a filament, the intensity does not vary and local scattering details cannot be resolved. Now, if incident illumination can be assumed locally constant (like in the case of distant light sources), the outgoing radiance $\mathrm{d}L(\varphi_i,\theta_i,h_o,\varphi_o,\theta_o)$ can be computed from (31). Integration with respect to incident direction ($\varphi_i$, $\theta_i$) yields:

$$L_o(h_o,\varphi_o,\theta_o) = \int_0^{2\pi}\int_{-\pi/2}^{\pi/2} f_{\mathrm{nearfield}} L_i \cos^2\theta_i \mathrm{d}\theta_i \mathrm{d}\varphi_i \tag{37}$$

with

$$f_{\mathrm{nearfield}}(\varphi_i,\theta_i,h_o,\varphi_o,\theta_o) = \int_{-1}^{1}\int_{-\infty}^{\infty} f_{\mathrm{BFSDF}}(\Delta s,h_i,\varphi_i,\theta_i,h_o,\varphi_o,\theta_o)\mathrm{d}\Delta s\mathrm{d}h_i. \tag{38}$$

A practical example of a near field scattering function for dielectric fibers is given in Section 9.2.

### 7.2 Curve Scattering with Locally Varying Incident Lighting

Although locally constant incident lighting may be assumed in most cases of direct illumination, this situation may change in case of indirect illumination. For the sake of completeness, we give the result for curve scattering with varying lighting too. For the rendering, integral one obtains:

$$\bar{L}_o(\varphi_o,\theta_o) = D\int_{-\infty}^{\infty}\int_{-1}^{1}\int_{0}^{2\pi}\int_{-\pi/2}^{\pi/2} f_{\mathrm{varyingCSDF}} L_i \cos^2\theta_i \mathrm{d}\theta_i\mathrm{d}\varphi_i\mathrm{d}h_i\mathrm{d}\Delta s \tag{39}$$

with

$$f_{\mathrm{varyingCSDF}}(\Delta s,h_i,\varphi_i,\theta_i,\varphi_o,\theta_o) = \frac{1}{2}\int_{-1}^{1} f_{\mathrm{BFSDF}}(\Delta s,h_i,\varphi_i,\theta_i,h_o,\varphi_o,\theta_o)\mathrm{d}h_o. \tag{40}$$

## 8 Previous Scattering Models

Especially in the context of hair rendering, several scattering models for light scattering from fibers have been proposed. We now show how they can be expressed in our notation which, for instance, allows systematic derivations of further scattering functions based on the corresponding BFSDF and BCSDF. Furthermore, we discuss their physical plausibility.

### 8.1 Kajiya and Kay's Model

One of the first simple approaches to render hair, which is still very commonly used, was presented by Kajiya and Kay [1]. It assumes a distant observer, since the outgoing radiance is constant over the width of a fiber and basically accounts for two scattering components: a scaled specular ad hoc Phong reflection at the surface of the fiber, centered over the specular cone, and an additional colored diffuse component. The diffuse coefficient $K_{\mathrm{diffuse}}$ is obtained from averaging the outgoing radiance of a diffuse BRDF over the illuminated width of the fiber, which produces significantly different results compared to the actual solution derived in Section 9.1.1 (see Fig. 11). The phenomenological Phong reflection fails to predict the correct intensities due to Fresnel reflectance (see Section 9.1.2).

Kajiya and Kay's model can be represented by a BCSDF as follows:

$$f_{\mathrm{BCSDF}}^{\text{Kajiya \& Kay}} = K_{\mathrm{Phong}}\frac{\cos^n(\theta_o+\theta_i)}{\cos\theta_i} + K_{\mathrm{diffuse}}. \tag{41}$$

### 8.2 The Model of Marschner et al. [2]

A much more sophisticated far field model for light scattering from hair fibers was proposed by Marschner

et al. [2]. It is based on significant measurements of light scattering from single hair filaments and implies again a distant observer and distant light sources. In [2], it is shown that all important features of light scattering from hairs can be basically explained by scattering from cylindrical dielectric fibers made of colored glass accounting for the first three scattering components (R, TT, TRT) introduced in Section 5 already. The BCSDF representing the basic model of Marschner et al. (without smoothing the caustic in the TRT component) can be directly derived from its underlying BFSDF, which is given by:

$$\begin{aligned} f_{\mathrm{BFSDF}}^{\mathrm{generatorMarschner}} = \\ \frac{\delta(h_o+h_i)}{\cos^2\theta_d}\Big(& g\Big(\theta_o+\theta_i-\Delta\theta_{\mathrm{R}}, w_{\mathrm{R}}^{\theta}\Big)a^{\mathrm{R}}(\theta_d,h_i) \\ & \delta(\Delta s)\delta\Big(\varphi_i-\lambda_{\varphi}^{\ \mathrm{R}}\Big) \\ & + g\Big(\theta_o+\theta_i-\Delta\theta_{\mathrm{TT}}, w_{\mathrm{TT}}^{\theta}\Big)a^{\mathrm{TT}}(\theta_d,h_i) \\ & \delta\Big(\Delta s-\lambda_s^{\mathrm{TT}}\Big)\delta\Big(\varphi_i-\lambda_{\varphi}^{\ \mathrm{TT}}\Big) \\ & + g\Big(\theta_o+\theta_i-\Delta\theta_{\mathrm{TRT}}, w_{\mathrm{TRT}}^{\theta}\Big)a^{\mathrm{TRT}}(\theta_d,h_i) \\ & \delta\Big(\Delta s-\lambda_s^{\mathrm{TRT}}\Big)\delta\Big(\varphi_i-\lambda_{\varphi}^{\mathrm{TRT}}\Big)\Big). \end{aligned} \tag{42}$$

This BFSDF can be seen as a generator for the basic model proposed in [2]. Note that it matches the BFSDF for a cylindric dielectric fiber with normalized Gaussians $g(x,w) := 1/(\sqrt{2\pi}w)\exp(-x/(2w^2))$ replacing the delta distributions $\delta_\theta$. This accounts for the fact that no fiber is perfectly smooth and the light is scattered to a finite lobe around the perfect specular cone. Additional shifts $\Delta\theta_{\mathrm{R,TT,TRT}}$ account for the tiled surface structure of hair fibers, which lead to shifted specular cones compared to a perfect dielectric fiber. For a better phenomenological match, in [2], it is furthermore proposed to replace $\theta_i$ with $\theta_d = (\theta_o-\theta_i)/2$. Hence, this BFSDF is just a variation of (15) and the complex derivation of the basic model (for a smooth fiber) given in [2] can be reduced to the following general recipe:

- Build a BFSDF by writing the scattering geometry in terms of products of delta functions with geometry terms $\lambda_\varphi$ and adding an additional attenuation factor.
- Derive the corresponding BCSDF according to (35). All ray density factors given in [2] as well as multiple scattering paths for the TRT-component are a direct consequence of the $\lambda_\varphi$-terms within the $\delta$-functions.

Note that, for performing the integration of $f_{\mathrm{BFSDF}}^{\mathrm{generatorMarschner}}$ in (35) symbolically, all delta functions of the form $\delta(\varphi_i - \lambda_\varphi^G(h_o))$ have to be transformed to make them directly dependent on the integration variable $h_o$. This is achieved by applying the following rule:

$$\int_{-1}^{1} f^G(h_o)\delta(\varphi_i-\lambda_\varphi^G(h_o))\mathrm{d}h_o = \sum_{i=0}^{n-1}\frac{f^G(h_o^i)}{\left|\frac{\mathrm{d}\lambda_\varphi^G}{\mathrm{d}h_o}(h_o^i)\right|}$$

with $G\in\{\mathrm{R},\mathrm{TT},\mathrm{TRT}\}$. Here, the expression $f^G(h_o)$ subsumes all factors depending on $h_o$ (except the $\delta$-function itself) and $h_o^i$ denotes the ith root of the expression $\varphi_i - \lambda_\varphi^G(h_o)$. For both the R and the TT component, there always exists exactly one root. For the TRT component, one needs a case differentiation since it exhibits either one or three roots. This exactly matches the observation of [2] that one or three different paths for rays of the TRT component occur. Although it is basically possible to compute the roots $h_o^i$ for all components directly, it is—for the sake of efficiency—useful to apply the approximation given by [2, (10)].

As an example, we now have a look at the direct surface reflection component (R-component). According to (42) one has:

$$\begin{aligned} f_{\mathrm{BFSDF}}^{\mathrm{R}} = & \frac{a^{\mathrm{R}}(\theta_d,h_i)}{\cos^2\theta_d} \\ & \delta(h_o+h_i)g(\theta_o+\theta_i-\Delta\theta_{\mathrm{R}}, w_{\mathrm{R}}^{\theta})\delta(\Delta s)\delta(\varphi_i-\lambda_\varphi^{\mathrm{R}}). \end{aligned}$$

Inserting this BFSDF into (35) for the corresponding BCSDF yields:

$$f_{\mathrm{BCSDF}}^{\mathrm{R}} = \frac{a^{\mathrm{R}}(\theta_d,\frac{\phi}{2})\cos(\frac{\phi}{2})g(\theta_o+\theta_i-\Delta\theta_{\mathrm{R}}, w_{\mathrm{R}}^{\theta})}{4\cos^2\theta_d}. \tag{43}$$

This equation matches the formula given in [2, (8)] (for $p=0$, inserting the ray density and attenuation factors).

Moreover, in [2], this basic BCSDF is extended to account for elliptic fibers and to smooth singularities in a post processing step. Since the BCSDF is computed for a perfect smooth cylinder, there are azimuthal angles $\phi_c$, for which the intensities of the TRT-components go to infinity. These singularities (caustics) are unrealistic and have to be smoothed out for real-world fibers. The method used in [2] is to first remove the caustics from the scattering distribution and to replace them by Gaussians (with roughly the same portion of energy) centered over the caustics positions. Four different parameters are needed to control this caustic removal process.

Note that this rather awkward caustic handling for the TRT component performed in [2] as well as a problematic singularity in the ray density factor of the TT-component for an index of refraction approaching the limit of one can be avoided; if another BFSDF for nonsmooth dielectric fibers is used, see Section 9.2.

Usually, hair has not a circular but an elliptic cross section geometry. Since even mild eccentricities $e$ especially influence the azimuthal appearance of the TRT component, this fact must not be neglected. In [2], the following simple approximation is proposed: Substitute an index $n^*$ for the original refractive index $n$ depending on $\varphi_h = (\varphi_i+\varphi_o)/2$ for the TRT-component as follows:

$$n^*(\varphi_h) = \frac{1}{2}((n_1+n_2)+\cos(2\varphi_h)(n_1-n_2)),$$

where

$$\begin{aligned} n_1 &= 2(n-1)e^2 - n + 2, \\ n_2 &= 2(n-1)e^{-2} - n + 2. \end{aligned}$$

## 9 Examples of Further Analytic Solutions and Approximations

In general, it cannot be expected that, for complex BFSDF/BCSDF, there are analytical solutions—a situation that is similar to the one for BSSRDF/BSDF. Nevertheless, in the following, we derive analytical solutions or at least analytical approximations for some interesting special cases.

### 9.1 Opaque Circular Symmetric Fibers

Perfectly opaque fibers with a circular cross section (like wires) can be modeled by a generalized cylinder together with a BRDF characterizing its surface reflectance. For this common case, we now show how both BFSDF and BCSDF can be derived. Since no internal light transport takes place, light is only reflected from a surface patch, if it is directly illuminated. Thus, the BFSDF simply writes as a product of the BRDF of the surface and two additional delta distributions limiting the reflectance to a single surface patch:

$$f_{\mathrm{BFSDF}} = f_{\mathrm{BRDF}}\delta(\xi_o - \xi_i)\delta(\Delta s), \tag{44}$$

or with respect to the other set of variables:

$$f_{\mathrm{BFSDF}} = f_{\mathrm{BRDF}}\delta(\phi + \arcsin h_o - \arcsin h_i)\delta(\Delta s) \tag{45}$$

with $\phi = M[\varphi_o - \varphi_i]$ being the relative azimuth. To derive the BCSDF, the complex (first) delta term has to be transformed into a form suitable for integration with respect to $h_i$ first. Applying the properties of Dirac distributions one obtains

$$\begin{aligned} f_{\mathrm{BFSDF}} = f_{\mathrm{BRDF}}&|\cos(\phi + \arcsin h_o)| \\ &\delta(h_i - \sin(\phi + \arcsin h_o))\delta(\Delta s). \end{aligned} \tag{46}$$

According to (35), for the BCSDF of a circular fiber mapped with an arbitrary BRDF, the following holds:

$$\begin{aligned} f_{\mathrm{BCSDF}} = &\frac{1}{2}\int_{-1}^{1}\int_{-1}^{1}\int_{-\infty}^{\infty} \\ &f_{\mathrm{BRDF}}|\cos(\phi + \arcsin h_o)| \\ &\delta(h_i - \sin(\phi + \arcsin h_o)) \\ &\delta(\Delta s)\mathrm{d}\Delta s\mathrm{d}h_i\mathrm{d}h_o \end{aligned} \tag{47}$$

$$\begin{aligned} = &\frac{1}{2}\int_{-1}^{\cos\phi} f_{\mathrm{BRDF}}|_{h_i=\sin(\phi+\arcsin h_o)} \\ &|\cos(\phi + \arcsin h_o)|\mathrm{d}h_o. \end{aligned} \tag{48}$$

Some exemplary results are shown in Fig. 11.

#### 9.1.1 Lambertian Reflectance

Many analytical BRDFs include a diffuse term accounting for Lambertian reflectance. The BCSDF approximation for such a Lambertian BRDF ($f_{\mathrm{BRDF}}^{\mathrm{Lambertian}} = k_d$) component can be directly calculated from (48):

$$f_{\mathrm{BCSDF}}^{\mathrm{Lambertian}} = \frac{k_d}{2}\int_{-1}^{\cos\phi}\cos(\phi + \arcsin h_o)\mathrm{d}h_o \tag{49}$$

with $k_d$ denoting the diffuse reflectance coefficient. To solve this integral, we replace the integrand by the absolute value of its Taylor series expansion about $h_o = 0$ up to an order of two:

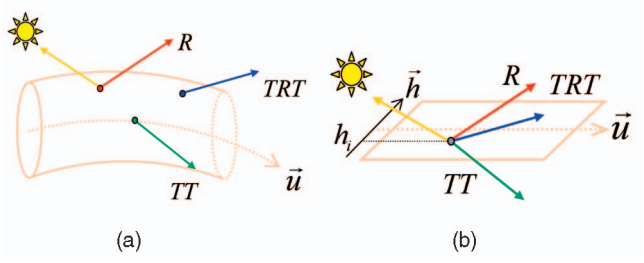


Fig. 8. A simple example of a position-dependent BSDF approximation for the BFSDF. (a) BFSDF snapshot of a perfect dielectric cylinder (R, TT, TRT). (b) Concentrating this BFSDF to the incident position gives a BSDF depending on the incident offset $h_i$ on a flat ribbon.

$$f_{\mathrm{BCSDF}}^{\mathrm{Lambertian}} \approx \frac{k_d}{2}\int_{-1}^{\cos\phi}\left|\cos\phi - h_o\sin\phi - \frac{h_o^2\cos\phi}{2}\right|\mathrm{d}h_o. \tag{50}$$

For the resulting approximative BCSDF, which has a relative error of less than five percent compared to the original, the following equation holds:

$$\begin{aligned} f_{\mathrm{BCSDF}}^{\mathrm{lambertian}} \approx &\frac{k_d}{2} \\ &\left|\frac{5}{6}\cos\phi + \cos^2\phi - \frac{1}{6}\cos^4\phi + \frac{1}{2}\sin\phi - \frac{1}{2}\sin\phi\cos^2\phi\right|. \end{aligned} \tag{51}$$

#### 9.1.2 Fresnel Reflectance

A second very important feature of opaque fibers like metal wires or coated plastics is Fresnel reflectance. We analyzed such a surface reflectance in the context of scattering from dielectric fibers in Section 5.1 (R-component) and the corresponding BCSDF was already derived in Section 8.2, see (43). In fact, if the BRDF is averaged over the width of a fiber, the BCSDF of a fiber with a narrow normalized reflection lobe BRDF (instead of a dirac delta distribution) can be very well approximated by this BCSDF for smooth fibers. Some exemplary scenes rendered with a combination of a Lambertian and a Fresnel BRDF can be seen in Fig. 11. The BCSDF approximation produces very similar results compared to the precise BRDF (BFSDF) solution, but requires much less computation time.

### 9.2 A Practical Parametric Near Field Shading Model for Dielectric Fibers with Elliptical Cross Sections

In the following, we derive a flexible and efficient near field shading model for dielectric fibers according to Section 7.1. This model accurately reproduces the scattering pattern for close ups but can be computed much more efficiently than the particle tracing (or an equivalent) that was typically used to capture the scattering pattern correctly.

As a basis, we take the three component BFSDF given in (42) that was also used to derive the BCSDF corresponding to the basic model proposed in [2], see Section 8.2. Due to surface roughness and inhomogeneities inside the fiber, the scattering distribution gets blurred (spatial and angular blurring), see Fig. 7. In order to account for this effect, we replace all $\delta$-distributions with special normalized Gaussians $g(I, x, w) := N(I, w)\exp(-x/(2w^2))$ with a normalization factor of $N(I, w) := 1/\int_{-I}^{I}\exp(-x/(2w^2))\mathrm{d}x$. The widths $w$ of these Gaussians

TABLE 1
Summary of All Parameters of the Near Field Shading Model

| notation | meaning |
|---|---|
| $\Delta\theta_{\mathrm{R,TT,TRT}}$ | longitudinal shifts of the specular cones |
| $w^{\theta}_{\mathrm{R,TT,TRT}}$ | widths for longitudinal blurring |
| $w^{\varphi}_{\mathrm{R,TT,TRT}}$ | widths for azimuthal blurring |
| $n$ | index of refraction |
| $\sigma$ | index of absorption |
| $k_d$ | diffuse coefficient |
| $e$ | eccentricity |

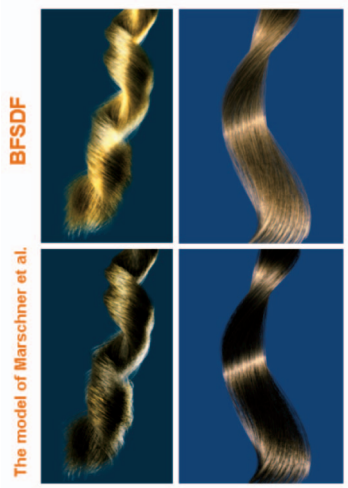


Fig. 9. Two different strands of light blond hair fibers. **Top row:** BFSDF Renderings with full global illumination. **Bottom row:** renderings of the same scenes according to Marschner et al. for direct (local) illumination. (The parameters were set to match our original BCSDF approximation of the BFSDF). This example clearly shows the evidence of multiple fiber scattering for the right perception of the hair color.

control the "strength of blurriness." Furthermore, we add a diffuse component approximating higher order scattering.

With these modifications, we obtain the following more general BFSDF for nonsmooth dielectric fibers:

$$
\begin{aligned}
f_{\mathrm{BFSDF}}^{\mathrm{dielectric}} = {} & \\
& \frac{g(1, h_o + h_i, w_h)}{\cos^2\theta_d}\Big(g\Big(\frac{\pi}{2}, \theta_o + \theta_i - \Delta\theta_{\mathrm{R}}, w^{\theta}_{\mathrm{R}}\Big)a^{\mathrm{R}}(\theta_d, h_i) \\
& \quad g(\infty, \Delta s, w_s)g\Big(\pi, \varphi_i - \lambda_{\varphi}{}^{\mathrm{R}}, w^{\mathrm{R}}_{\varphi}\Big) \\
& \quad + g\Big(\frac{\pi}{2}, \theta_o + \theta_i - \Delta\theta_{\mathrm{TT}}, w^{\theta}_{\mathrm{TT}}\Big)a^{\mathrm{TT}}(\theta_d, h_i) \\
& \quad g\Big(\infty, \Delta s - \lambda_s^{\mathrm{TT}}, w_s\Big)g\Big(\pi, \varphi_i - \lambda_{\varphi}{}^{\mathrm{TT}}, w^{\mathrm{TT}}_{\varphi}\Big) \\
& \quad + g\Big(\frac{\pi}{2}, \theta_o + \theta_i - \Delta\theta_{\mathrm{TRT}}, w^{\theta}_{\mathrm{TRT}}\Big)a^{\mathrm{TRT}}(\theta_d, h_i) \\
& \quad g\Big(\infty, \Delta s - \lambda_s^{\mathrm{TRT}}, w_s\Big)g\Big(\pi, \varphi_i - \lambda_{\varphi}^{\mathrm{TRT}}, w^{\mathrm{TRT}}_{\varphi}\Big)\Big) \\
& + k_d\delta(\Delta s).
\end{aligned}
\tag{52}
$$

Note that the awkward caustic handling done in [2] can be avoided by calculating the corresponding BCSDF out of $f_{\mathrm{BFSDF}}^{\mathrm{dielectric}}$, see Section 8.2. Here, the appearance of the caustics is fully determined by the azimuthal blurring width $w^{\varphi}_{\mathrm{TRT}}$. The more narrow this width is, the closer the caustic pattern matches the one of a smooth fiber. All azimuthal scattering of such a BCSDF can be derived efficiently by numerical integration in a preprocessing pass. The result is a two-dimensional lookup table with respect to $\theta_d$ and $\varphi$, which is then used for rendering and which replaces the complex computations proposed in Section 8.2. Some exemplary comparisons between BFSDF and BCSDF-renderings are presented in the Appendix (Fig. 10).


Fig. 10. Different strands of translucent dielectric fibers illuminated by three distant point light sources. The two left-most images were rendered with a hair like material and the two rightmost images show synthetic fibers. Direct illumination was computed according to Section 9.2. The BCSDF was computed from the BFSDF for dielectric fibers ((52)).

Assuming locally constant illumination, a near field scattering function $f_{\mathrm{nearfield}}^{\mathrm{dielectric}}$ can be derived from the BFSDF by solving (38) in Section 7.1 for $f_{\mathrm{BFSDF}}^{\mathrm{dielectric}}$. Assuming a narrow width $w_h$, i.e., a small spatial blurring, this approximately yields:

$$
\begin{aligned}
f_{\mathrm{nearfield}}^{\mathrm{dielectric}} = {} & 2k_d \\
& + \frac{1}{\cos^2\theta_d}\Big(g\Big(\frac{\pi}{2}, \theta_o + \theta_i - \Delta\theta_{\mathrm{R}}, w^{\theta}_{\mathrm{R}}\Big)a^{\mathrm{R}}(\theta_d, h_o) \\
& \quad g\Big(\pi, \phi + 2\arcsin h_o, w^{\mathrm{R}}_{\varphi}\Big) \\
& \quad + g\Big(\frac{\pi}{2}, \theta_o + \theta_i - \Delta\theta_{\mathrm{TT}}, w^{\theta}_{\mathrm{TT}}\Big)a^{\mathrm{TT}}(\theta_d, h_o) \\
& \quad g\Big(\pi, \phi + M[\pi + 2\arcsin h_o - 2\arcsin(h_o/n')], w^{\mathrm{TT}}_{\varphi}\Big) \\
& \quad + g\Big(\frac{\pi}{2}, \theta_o + \theta_i - \Delta\theta_{\mathrm{TRT}}, w^{\theta}_{\mathrm{TRT}}\Big)a^{\mathrm{TRT}}(\theta_d, h_o) \\
& \quad g\Big(\pi, \phi + 4\arcsin(h_o/n') - 2\arcsin h_o, w^{\mathrm{TRT}}_{\varphi}\Big)\Big).
\end{aligned}
\tag{53}
$$

This result can be directly used for the shading of fibers with a circular cross section. Although elliptic fibers could be modeled by calculating the corresponding $\lambda$ terms, we propose using the following more efficient approximation instead: Change the diameter of the primitive used for rendering (a half cylinder or a flat polygon) according to the projected diameter and apply the first order approximation for mild eccentricities proposed in [2] (see Section 8.2).

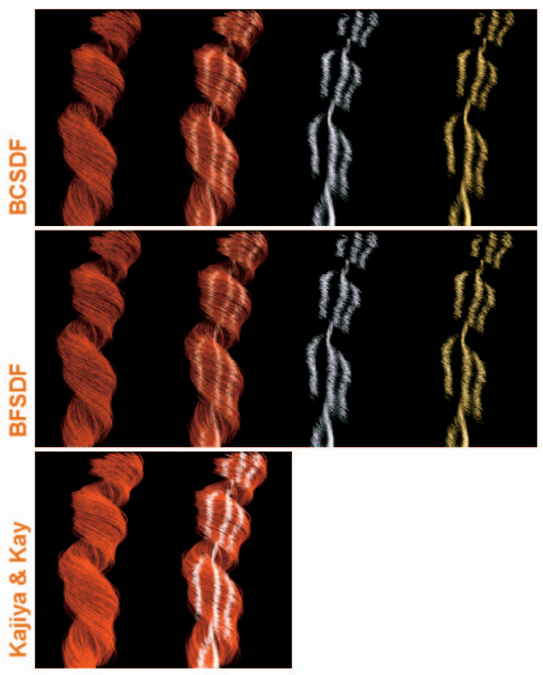


Fig. 11. **Top row:** Various physically-based (i.e., energy conserving) BCSDF renderings of opaque fibers illuminated by three distant point light sources. The BCSDFs were generated according to Section 9.1 from the following BRDF types: Lambertian (*left*); $\mathrm{Fresnel} + (1 - \mathrm{Fresnel}) \times \mathrm{Lambertian}$ (*left middle*); Fresnel for aluminium (*right middle*); Fresnel for gold (*right*). These BCSDF examples are given in a purely analytical form, so that parameters—like index of refraction—can be easily changed on the fly, e.g., for the "gold" and "aluminium" examples, which use the same BCSDF with different material properties. **Middle row:** BFSDF renderings of the same scenes. Notice how well the BCSDF renderings already match the BFSDF renderings. **Bottom row:** Some exemplary renderings with the phenomenological model of Kajiya and Kay. Lighting and geometry was not changed. The diffuse component was computed according to [1] from the diffuse coefficient of the BRDF. The width of the specular lobe (if present) as well the peak intensity was set to match the ones of the original physically-based renderings setting the Fresnel factor to one. Nevertheless, the results differ substantially from the BCSDF, respectively, BFSDF renderings. Note that the BCSDF images were computed approximately one order of magnitude faster, since $16\times$ less eye-rays per pixel were needed to achieve a similar rendering quality.

Results obtained with this model are (Figs. 10, 11, 12, 13, 14, and 15). Notice especially the results shown in Fig. 14, in which comparisons to photographs are given showing how well the scattering patterns of the renderings are matching the originals.

Interestingly, this near field shading model is computationally less expensive than the far field model of [2]. It can be evaluated more than twice as fast (per call) compared to an efficient reimplementation of this far field model. Furthermore, an extension of the model to all higher order scattering components is possible, since analytical expressions for corresponding geometry terms $\lambda$ are available. A summary of all parameters of the model is given in Table 1.

## 10 Integration into Existing Rendering Systems

Existing rendering kernels can cope with BSDF and polygons only. Therefore, we propose approximations of the BFSDF, which translate it to some position dependent BSDF and preserve subtle scattering details.

Fig. 12. Various BFSDF rendering results.

### 10.1 BSDF Approximation of the BFSDF

In most cases, internal light transport is limited to a very small region around the incident position. Furthermore, the diameter of a typical fiber is very small compared to other dimensions of a scene. Hence, concentrating the BFSDF to the infinitesimal surface patch in which incident light penetrates the fiber introduces only very few inaccuracies (see Fig. 8). This approach may be formalized by integrating an BFSDF with respect to $\Delta s$ and $\xi_o$:

$$f_{\mathrm{BSDF}}[h_i](\varphi_i, \theta_i, \varphi_o, \theta_o) := \int_{-\infty}^{\infty} \int_{0}^{2\pi} f_{\mathrm{BFSDF}} \mathrm{d}\xi_o \mathrm{d}\Delta s. \qquad (54)$$

The result is some position-dependent BSDF $f_{\mathrm{BSDF}}[h_i](\varphi_i, \theta_i, \varphi_o, \theta_o)$ varying over the width of the fiber. With this approximation, a fiber can be modeled very well by a primitive having the same effective cross section like the minimum enclosing cylinder, e.g., flat ribbons or half cylinders always facing the light and camera.

### 10.2 BCSDF as BSDF

If the BCSDF is used for rendering, its transformation to a BSDF is trivial: In fact, nothing has to be changed. Only diameter $D$ has to be neglected in the rendering integral if the fibers are modeled by primitives geometrically accounting for their effective cross sections.

## 11 Indirect Illumination and Multiple Scattering

For light colored fibers, indirect illumination—mostly due to multiple fiber scattering—significantly contributes to the overall scattering distribution and must not be neglected. For an example, we refer to [3], which addresses the importance

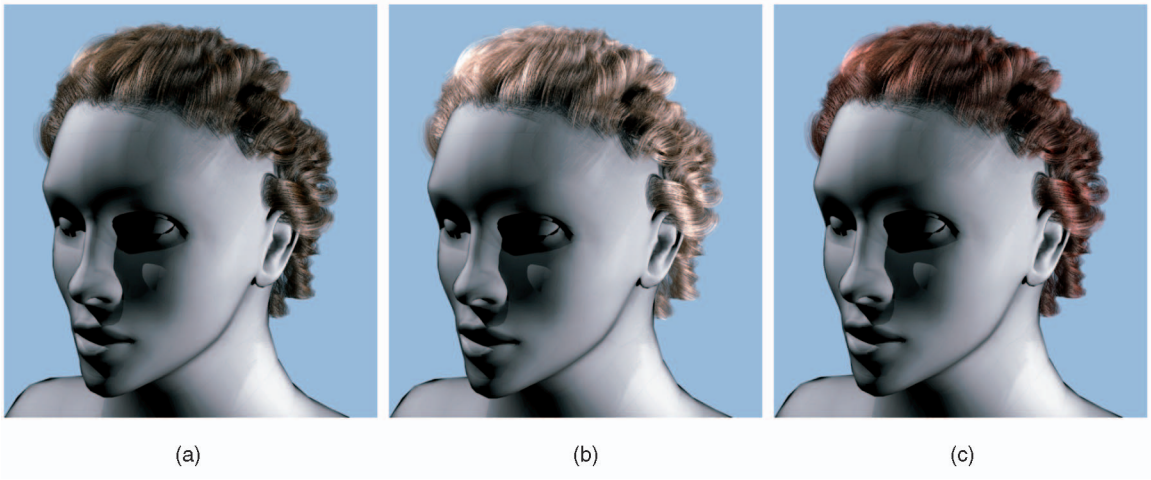


Fig. 13. BFSDF renderings of a hairstyle consisting of about 90,000 individual hair fibers ((a) brown, (b) blond, and (c) dark red dyed) illuminated by five point light sources.

of global illumination in case of blond hair. A Monte Carlo rendering of light blond hair is presented in Fig. 9.

Because a BFSDF already comprises all internal light transport of a single filament, no further simulation of internal scattering has to be performed. Therefore, sampling a BFSDF for multiple filament scattering is more efficient than simulating the entire filament scattering—including internal light transport–during rendering.

However, although global illumination due to multiple fiber scattering can be basically accelerated by sampling the BFSDF—see Section 10—this direct approach may still be impracticable with respect to rendering time.

Especially in the field of interactive hair rendering, several very efficient rendering techniques—such as deep or opacity shadow maps and pixel blending—have been proposed to approximate effects of multiple fiber scattering [20], [21], [22], [23]. In a forthcoming publication, we will show how our theoretical framework can be applied to obtain physically-based results using these techniques.

Fig. 14. An oval made of rough plastic illuminated by one point light source. The upper row shows photographs and the second row renderings with a variant of the shader presented in Section 9.2. The parameters are set to roughly match the original photographs. Note the similarity of both positions and intensities of the highlights for different viewing angles. It took less than five seconds to render each frame with simple ray tracing.

## 12 Conclusion and Future Work

In this paper, we derived a novel theoretical frame work for efficiently computing light scattering from filaments. In contrast to previous approaches developed in the realm of hair rendering, it is much more flexible and can handle many types of filaments and fibers like hair, fur, ropes, and wires. Approximations for different levels of (geometrical) abstraction can be derived in a straightforward way. Furthermore, our approach provides a firm basis for comparisons and classifications of filaments with respect to their scattering properties. The basic idea was to adopt basic radiometric concepts like BSSRDF and BSDF to the realm of fiber rendering. Although the resulting radiance transfer functions are, strictly speaking, valid for infinite fibers only, they can be seen as suitable local approximations.

Different types of scattering functions for filaments were derived and parameterized with respect to the minimum enclosing cylinder. The Bidirectional Fiber Scattering Distribution Function (BFSDF) basically describes the radiance transfer at this enclosing cylinder. It is an abstract optical property of a filament which can be estimated by measurement, simulation, or analysis of the scattering distribution of a single filament. The BFSDF can be seen as the basis for all further approximations, see Fig. 1. We believe that we have derived scattering functions for most of the special cases that will occur in practice. For examples of rendering results based on various of the derived scattering functions, we refer to the Appendix.

However, the theoretical analysis given in this paper should be seen as a starting point and further work is required to investigate many important problems which arise in the case of very complex "real-world filaments" such as global illumination for fiber-based geometries. As an example, we refer to [3] where the importance of multiple fiber scattering for light colored hair was addressed. It plays an important role for the right perception of the hair color and must not be neglected (see also Fig. 9). Efficient compression strategies are needed since the BFSDF is an eight-dimensional function such as the general BSSRDF. Moreover, if the BFSDF is given in a purely numerical form, the four-dimensional rendering integral itself is very costly to evaluate. Therefore, the BFSDF should be approximated by series of analytical functions

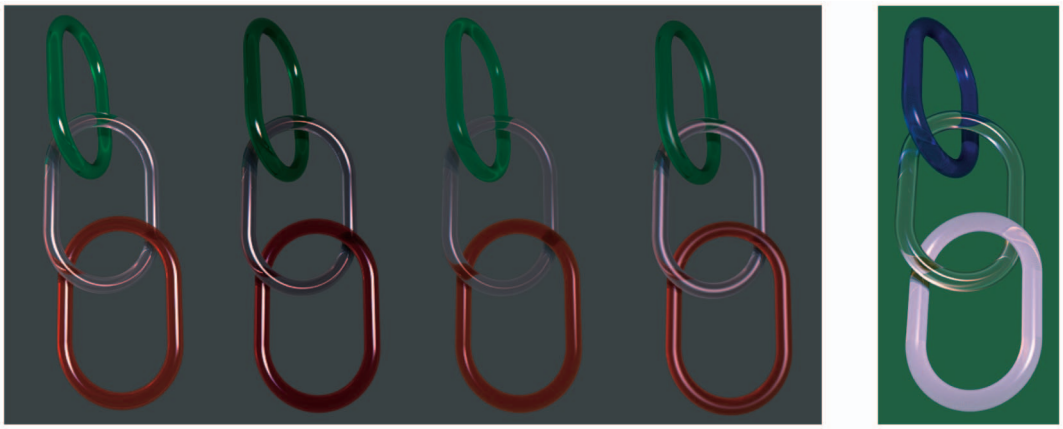

Fig. 15. Various BFSDF examples with a more complex illumination. The images were rendered in about 30 seconds each.

which can be efficiently integrated. Fortunately, many scattering distributions have very few intensity peaks which can be well approximated with existing compression schemes (e.g., Lafortune Lobes [24], Reflectance Field Polynomials [25], Linear Basis Decomposition [26], and clustering and factorization [27], [28], [29]) developed in the realm of BRDF and BTF rendering.

Another important challenge is the reconstruction of the BFSDF or BCSDF from macroscopic image data, which frequently are more easily obtainable than systematic measurements at the fiber level. We presume that using special modeling knowledge which is coded by the usage of a lower dimensional scattering functions such as the BCSDF might be crucial for the practical solvability of inverse problems involving the BFSDF.

## APPENDIX

All renderings given in the Appendix or as supplemental material are rendered with a proprietary ray tracer.

Unless stated differently, "BFSDF rendering" always means that, for direct illumination, the near-field shader (see Section 9.2) was used and indirect illumination was computed from an importance-sampled BFSDF using Monte-Carlo path tracing.

## ACKNOWLEDGMENTS

The authors are grateful to the anonymous referees for their many detailed suggestions. They would like to thank R. Klein for the opportunity to use a robot camera system for the photographs given in Fig. 14, and to R. Sarlette and A. Hennes for their technical support. The presented work is partially supported by *Deutsche Forschungsgemeinschaft* under grant We 1945/3-2.

## REFERENCES

[1] J.T. Kajiya and T.L. Kay, "Rendering Fur with Three Dimensional Textures," *Proc. 16th Ann. Conf. Computer Graphics and Interactive Techniques,* pp. 271-280, 1989, http://doi.acm.org/10.1145/74333.74361.

[2] S.R. Marschner, H.W. Jensen, M. Cammarano, S. Worley, and P. Hanrahan, "Light Scattering from Human Hair Fibers," *ACM Trans. Graphics,* vol. 22, no. 3, pp. 780-791, 2003, http://doi.acm.org/10.1145/882262.882345.

[3] A. Zinke, G. Sobottka, and A. Weber, "Photo-Realistic Rendering of Blond Hair," *Proc. Vision, Modeling, and Visualization,* B. Girod, M. Magnor, and H.-P. Seidel, eds., pp. 191-198, Nov. 2004.

[4] D.B. Goldman, "Fake Fur Rendering," *Proc. 24th Ann. Conf. Computer Graphics and Interactive Techniques (SIGGRAPH '97),* pp. 127-134, 1997, http://doi.acm.org/10.1145/258734.258807.

[5] T.-Y. Kim, "Modeling, Rendering and Animating Human Hair," PhD thesis, Dept. of Computer Science, Univ. of Southern California, Dec. 2002.

[6] F.E. Nicodemus, J.C. Richmond, J.J. Hsia, I.W. Ginsberg, and T. Limperis, *Geometric Considerations and Nomenclature for Reflectance,* vol. 161, Nat'l Bureau of Standards (US), 1977.

[7] H.W. Jensen, S.R. Marschner, M. Levoy, and P. Hanrahan, "A Practical Model for Subsurface Light Transport," *Proc. 28th Ann. Conf. Computer Graphics and Interactive Techniques (SIGGRAPH '01),* pp. 511-518, 2001, http://doi.acm.org/10.1145/383259.383319.

[8] T. Mertens, J. Kautz, P. Bekaert, F.V. Reeth, and T.H.-P. Seidel, "Efficient Rendering of Local Subsurface Scattering," *Proc. Pacific Conf. Computer Graphics and Applications,* 2003.

[9] K.J. Dana, B. van Ginneken, S.K. Nayar, and J.J. Koenderink, "Reflectance and Texture of Real-World Surfaces," *Proc. IEEE Conf. Computer Vision and Pattern Recognition,* pp. 151-157, 1997.

[10] V.L. Volevich, E.A. Kopylov, A.B. Khodulev, and O.A. Karpenko, "The 7th International Conference on Computer Graphics and Visualization," *Proc. Eurographics Symp. Rendering,* 1997.

[11] E. Gröller, R.T. Rau, and W. Strasser, "Modeling and Visualization of Knitwear," *IEEE Trans. Visualization and Computer Graphics,* vol. 1, no. 4, pp. 302-310, Oct.-Dec. 1995.

[12] Y.-Q. Xu, Y. Chen, S. Lin, H. Zhong, E. Wu, B. Guo, and H.-Y. Shum, "Photorealistic Rendering of Knitwear Using the Lumislice," *Proc. 28th Ann. Conf. Computer Graphics and Interactive Techniques (SIGGRAPH '01),* pp. 391-398, 2001.

[13] N. Adabala, N. Magnenat-Thalmann, and G. Fei, "Real-Time Visualization of Woven Textiles," *Publication of EUROSIS,* J.C. Guerri, P.A, and C.A. Palau, eds., pp. 502-508, 2003.

[14] C.L. Adler, J.A. Lock, B.R. Stone, and C.J. Garcia, "High-Order Interior Caustics Produced in Scattering of a Diagonally Incident Plane Wave by a Circular Cylinder," *Optical Soc. Am.,* vol. 14, 1996.

[15] C.L. Adler, J.A. Lock, and B.R. Stone, "Rainbow Scattering by a Cylinder with a Nearly Elliptical Cross Section," *Optical Soc. Am.,* 1998.

[16] C.L. Adler, D. Phipps, K.W. Saunders, J.K. Nash, and J.A. Lock, "Supernumerary Spacing of Rainbows Produced by an Elliptical-Cross-Section Cylinder," *Optical Soc. Am.,* 2001.

[17] C.M. Mount, D.B. Thiessen, and P.L. Marston, "Scattering Observations for Tilted Transparent Fibers: Evolution of Airy Caustics with Cylinder Tilt and the Caustic Merging Transition," *Applied Optics,* vol. 37, no. 9, pp. 243-249, 1998.

[18] L. Mees, K.F. Ren, G. Grehan, and G. Gouesbet, "Scattering of a Gaussian Beam by an Infinite Cylinder with Arbitrary Location and Arbitrary Orientation: Numerical Results," *Optical Soc. Am.,* 1998.

[19] R. Schuh and T. Wriedt, "Light Scattering from Bent Cylindrical Fibers for Fiber Length and Diameter Characterization," *Particle & Particle Systems Characterization,* vol. 20, pp. 243-249, 2003.

[20] T. Lokovic and E. Veach, "Deep Shadow Maps," *Proc. 27th Ann. Conf. Computer Graphics and Interactive Techniques (SIGGRAPH '00)*, pp. 385-392, 2000, http://doi.acm.org/10.1145/344779.344958.
[21] C. Dachsbacher and M. Stamminger, "Translucent Shadow Maps," *Proc. 14th Eurographics Workshop Rendering (EGRW '03)*, pp. 197-201, 2003.
[22] T. Mertens, J. Kautz, P. Bekaert, and F.V. Reeth, "A Self-Shadow Algorithm for Dynamic Hair Using Density Clustering," *Proc. Eurographics Symp. Rendering*, 2004.
[23] T.-Y. Kim and U. Neumann, "Opacity Shadow Maps," *Proc. Eurographics Rendering Workshop*, pp. 177-182, 2001.
[24] K. Daubert, H. Lensch, W. Heidrich, and H.-P. Seidel, "Efficient Cloth Modeling and Rendering," *Proc. 12th Eurographics Workshop Rendering*, pp. 63-70, 2001.
[25] J. Meseth, G. Müller, and R. Klein, "Reflectance Field Based Real-Time, High-Quality Rendering of Bidirectional Texture Functions," *Computers and Graphics*, vol. 28, no. 1, pp. 103-112, Feb. 2004.
[26] W. Matusik, H. Pfister, A. Ngan, P. Beardsley, R. Ziegler, and L. McMillan, "Image-Based 3D Photography Using Opacity Hulls," *Proc. 29th Ann. Conf. Computer Graphics and Interactive Techniques (SIGGRAPH '02)*, pp. 427-437, 2002, http://doi.acm.org/10.1145/566570.566599.
[27] J. Kautz and M. McCool, "Interactive Rendering with Arbitrary BRDFs Using Separable Approximations," *Proc. 10th Eurographics Workshop Rendering*, pp. 281-292, 1999.
[28] X. Liu, Y. Hu, J. Zhang, X. Tong, B. Guo, and H.-Y. Shum, "Synthesis and Rendering of Bidirectional Texture Functions on Arbitrary Surfaces," *IEEE Trans. Visualization and Computer Graphics*, vol. 10, no. 3, pp. 278-289, May-June 2004.
[29] M. Sattler, R. Sarlette, and R. Klein, "Efficient and Realistic Visualization of Cloth," *Proc. 14th Eurographics Workshop Rendering (EGRW '03)*, pp. 167-177, 2003.

**Arno Zinke** received the MSc degree in computer science (Dipl.-Inform.) from the University of Bonn, Germany, in 2004, where he is currently pursuing the PhD degree in computer science. His research interests include physically-based simulation and rendering.

**Andreas Weber** received the MSc degree in mathematics (Dipl.-Math.) in 1990 and the PhD degree (Dr. rer. nat.) in computer science in 1993 from the University of Tübingen, Germany. After being a postdoctoral researcher at the University of Tübingen, Germany, Cornell University, Ithaca, New York, and the Fraunhofer-Institut for Computer Graphics, Darmstadt, Germany, he joined the University of Bonn, Germany, as a professor of computer science. He has published more than 50 research papers in computer graphics and computer algebra. A focus of his current research is physics-based simulation and animation. He is a member of the IEEE.